

Article

Comparative Evaluation of Commercial, Freely Available, and Open-Source Tools for Single-Cell Analysis Within Freehand-Defined Histological Brightfield Image Regions of Interest

Filippo Piccinini ^{1,2}, Marcella Tazzari ¹, Maria Maddalena Tumedei ¹, Nicola Normanno ¹,
Gastone Castellani ^{2,3} and Antonella Carbonaro ^{4,*}

¹ IRCCS Istituto Romagnolo per lo Studio dei Tumori (IRST) “Dino Amadori”, Via Piero Maroncelli 40, 47014 Meldola, Italy; filippo.piccinini@irst.emr.it (F.P.); marcella.tazzari@irst.emr.it (M.T.); maria.tumedei@irst.emr.it (M.M.T.); nicola.normanno@irst.emr.it (N.N.)

² Department of Medical and Surgical Sciences (DIMEC), University of Bologna, Via G. Massarenti 9, 40138 Bologna, Italy; gastone.castellani@unibo.it

³ IRCCS Azienda Ospedaliero-Universitaria di Bologna S. Orsola, Via G. Massarenti 9, 40138 Bologna, Italy

⁴ Department of Computer Science and Engineering (DISI), University of Bologna, Bologna, Via dell’Università 50, 47521 Cesena, Italy

* Correspondence: antonella.carbonaro@unibo.it

Abstract: In the field of histological analysis, one of the typical issues is the analysis of single cells contained in regions of interest (i.e., ROIs). Today, several commercial, freely available, and open-source software options are accessible for this task. However, the literature lacks recent extensive reviews that summarise the functionalities of the opportunities currently available and provide guidance on selecting the most suitable option for analysing specific cases, for instance, irregular freehand-defined ROIs on brightfield images. In this work, we reviewed and compared 14 software tools tailored for single-cell analysis within a 2D histological freehand-defined image ROI. Precisely, six open-source tools (i.e., *CellProfiler*, *Cytomine*, *Digital Slide Archive*, *Icy*, *ImageJ/Fiji*, *QuPath*), four freely available tools (i.e., *Aperio ImageScope*, *NIS Elements Viewer*, *Sedeen*, *SlideViewer*), and four commercial tools (i.e., *Amira*, *Arivis*, *HALO*, *Imaris*) were considered. We focused on three key aspects: (a) the capacity to handle large file formats such as SVS, DICOM, and TIFF, ensuring compatibility with diverse datasets; (b) the flexibility in defining irregular ROIs, whether through automated extraction or manual delineation, encompassing square, circular, polygonal, and freehand shapes to accommodate varied research needs; and (c) the capability to classify single cells within selected ROIs on brightfield images, ranging from fully automated to semi-automated or manual approaches, requiring different levels of user involvement. Thanks to this work, a deeper understanding of the strengths and limitations of different software platforms emerges, facilitating informed decision making for researchers looking for a tool to analyse histological brightfield images.

Keywords: brightfield microscopy; image processing; single-cell analysis; histology; oncology



Academic Editor: Tamás Haidegger

Received: 23 December 2024

Revised: 26 February 2025

Accepted: 3 March 2025

Published: 7 March 2025

Citation: Piccinini, F.; Tazzari, M.; Tumedei, M.M.; Normanno, N.; Castellani, G.; Carbonaro, A. Comparative Evaluation of Commercial, Freely Available, and Open-Source Tools for Single-Cell Analysis Within Freehand-Defined Histological Brightfield Image Regions of Interest. *Technologies* **2025**, *13*, 110. <https://doi.org/10.3390/technologies13030110>

Copyright: © 2025 by the authors. Licensee MDPI, Basel, Switzerland. This article is an open access article distributed under the terms and conditions of the Creative Commons Attribution (CC BY) license (<https://creativecommons.org/licenses/by/4.0/>).

1. Introduction

Recent advancements in histopathology have been driven by innovations in digital imaging and computational analysis [1]. A critical area of focus is evaluating single-cell data within specific regions of interest (ROIs) from high-resolution histological images, particularly for cancer research, immunohistochemistry (IHC), and tissue microenvironment

studies. The ability to accurately identify and quantify individual cells within a defined ROI even in a simple brightfield image has significant implications for diagnosis, prognosis, and therapeutic decisions [2]. In fact, it is worth noting that brightfield images are currently used for several pre-clinical and clinical analyses. For instance, multiplexed bright-field methodologies and platforms are, today, the reference for the analysis of predictive markers for immunotherapy [3].

The rise of two-dimensional (2D) whole slide imaging (WSI) and the need for efficient, scalable tools to manage, analyse, and interpret these large datasets has led to the development of various software platforms [4]. These platforms range from commercial to open-source solutions [5], from generalist [6] to specific tools [7], and offer distinct features to accommodate the increasing complexity of modern histological analysis [8]. Despite the availability of such tools, there is a critical need for a comprehensive comparison to guide researchers in selecting the most appropriate software for specific tasks, particularly those involving single-cell analysis within freehand-selected histological ROIs on brightfield images. For example, the authors in [5] recently discussed the growing role of artificial intelligence (AI) in the field of digital pathology, introducing some open-source segmentation tools and analysing their usage and customisation in histological imaging. Similarly, the authors in [9] examined the latest AI and deep learning (DL) techniques for cell analysis and data mining in microscopy images. It is important to note that whilst most available tools permit rectangular ROI selection, very few allow for true irregular freehand selection, and many are optimised for fluorescent images rather than classical widefield brightfield microscopy [10].

This study provides a detailed evaluation of 14 popular tools, encompassing commercial, freely available, and open-source solutions. Specifically, six open-source tools (i.e., *CellProfiler* [11], *Cytomine* [12], *Digital Slide Archive* [13], *Icy* [14], *ImageJ/Fiji* [15,16], *QuPath* [17]), four freely available tools (i.e., *Aperio ImageScope*, *NIS Elements Viewer*, *Sedeen*, *SlideViewer*), and four commercial tools (i.e., *Amira*, *Arivis*, *HALO*, *Imaris*) have been considered. The evaluation focuses on aspects important to researchers, including the ability to handle large file formats (e.g., scanner vendor-specific format—SVS, digital imaging and communications in medicine—DICOM, tagged image file format—TIFF), flexibility in defining and extracting ROIs, and the functionality for classifying single cells on brightfield images using automated, semi-automated, or manual techniques.

In this work, a benchmark analysis was conducted using a representative irregular freehand-defined ROI from a brightfield WSI red, green, and blue (RGB) case, providing quantitative insights into the performance of currently available software tools. Notably, most of these tools are originally designed for multi-channel images, the most common image type in the fluorescence domain. Although brightfield multi-channel immunohistochemistry images can be generated by sequentially staining the sample [18], or through multispectral imaging in the range of the visible light [19], we focused the present study on the most prevalent case in brightfield microscopy, the RGB image type [20]. The results indicate that several tools now offer highly accurate solutions. For example, the open-source software *QuPath* stands out for its comprehensive feature set, comparable to those provided by commercial solutions with annual costly license fees ranging from a few thousand to EUR 25,000, depending on the desired configuration and service. However, it is important to note that evaluating the commercial tools was challenging due to the restricted functionality of the testing license. As such, the reported performance values can be considered a lower bound, with potential for improvement under unrestricted conditions. In conclusion, this analysis serves as a valuable guide to the current options available for single-cell histological analysis, helping researchers better understand what to expect for their specific analytical needs.

The remainder of this article is structured as follows: Section 2 provides a detailed overview of the single-cell analysis tools available today. Section 3 presents a qualitative comparison of the different tools, focusing on performance in handling large datasets and the capabilities of defining ROIs and conducting automated analysis. Section 4 introduces the case study used for the quantitative comparison of the tools, with the results and discussion following in Section 5. Finally, Section 6 concludes the paper by summarising the key findings and offering recommendations for researchers seeking to select the most suitable tool for analysing brightfield images.

2. Description of the Tools

In this study, we analysed the different tools available today for single-cell analysis within a 2D histological WSI ROI. These tools were categorised into three groups. (a) Open-source tools (six tools, Figure 1) included *CellProfiler*, *Cytomine*, *Digital Slide Archive*, *Icy*, *ImageJ/Fiji*, and *QuPath*. (b) Freely available tools (four tools, Figure 2) included *Aperio ImageScope*, *NIS Elements Viewer*, *Sedeen*, and *SlideViewer*. (c) Commercial tools (four tools, Figure 3) included *Amira*, *Arivis*, *HALO*, and *Imaris*. What follows is a brief description of the key functionalities and strengths of each tool:

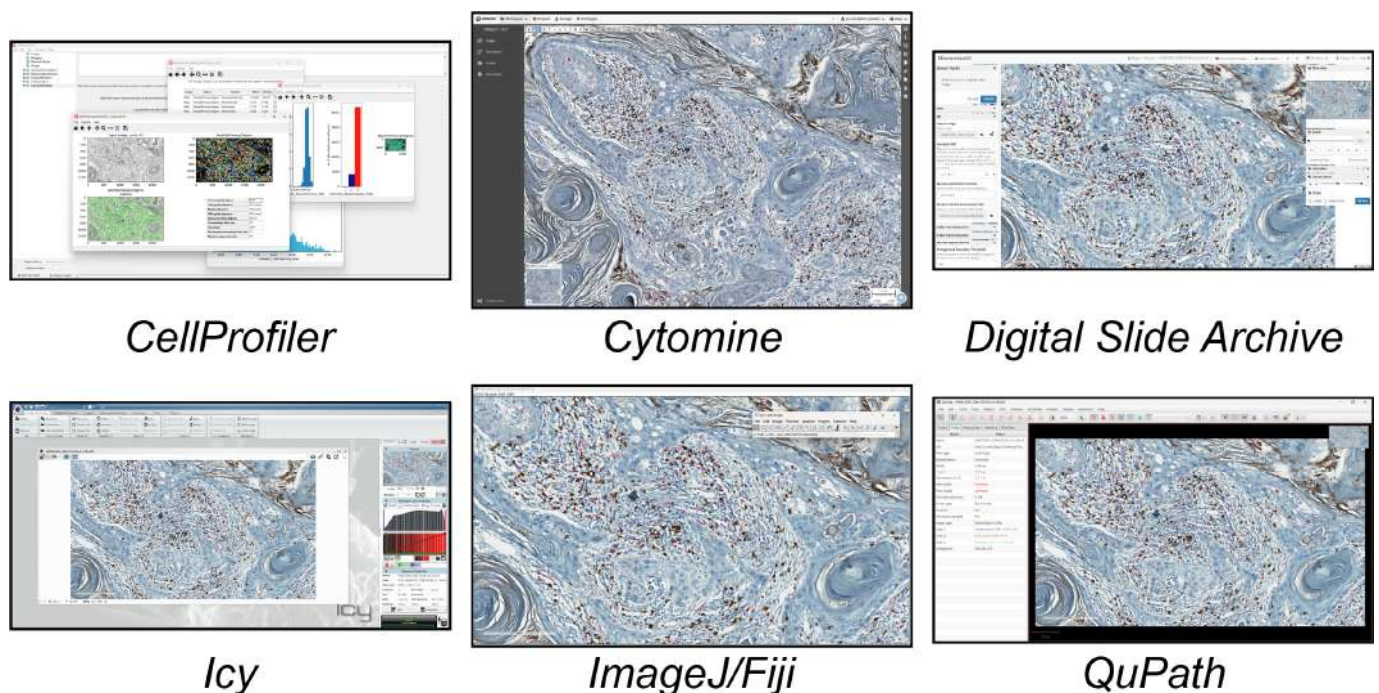


Figure 1. Main GUI of different open-source single-cell analysis tools. From top to bottom and left to right: *CellProfiler*, *Cytomine*, *Digital Slide Archive*, *Icy*, *ImageJ/Fiji*, and *QuPath*.

2.1. Open-Source Tools

CellProfiler (<https://cellprofiler.org/>) [11]: *CellProfiler*, originally developed in *MATLAB* in 2005 [21], is an open-source software with a graphical user interface (GUI) that was improved using *Java* and *Python* languages. It supports modular and scalable image processing. Through its GUI, users can construct an image analysis pipeline by assembling a series of functional modules, each responsible for a different task. These modules can be tailored to specific experimental needs by adjusting the parameters. The software is widely used in cellular and molecular biology studies, where the precise quantification of cell morphology, fluorescence intensity, or subcellular structures is required. While *CellProfiler* provides an intuitive interface for users without coding expertise, more advanced users

can further extend its functionalities through integration with external tools such as *ImageJ* and *Python*.

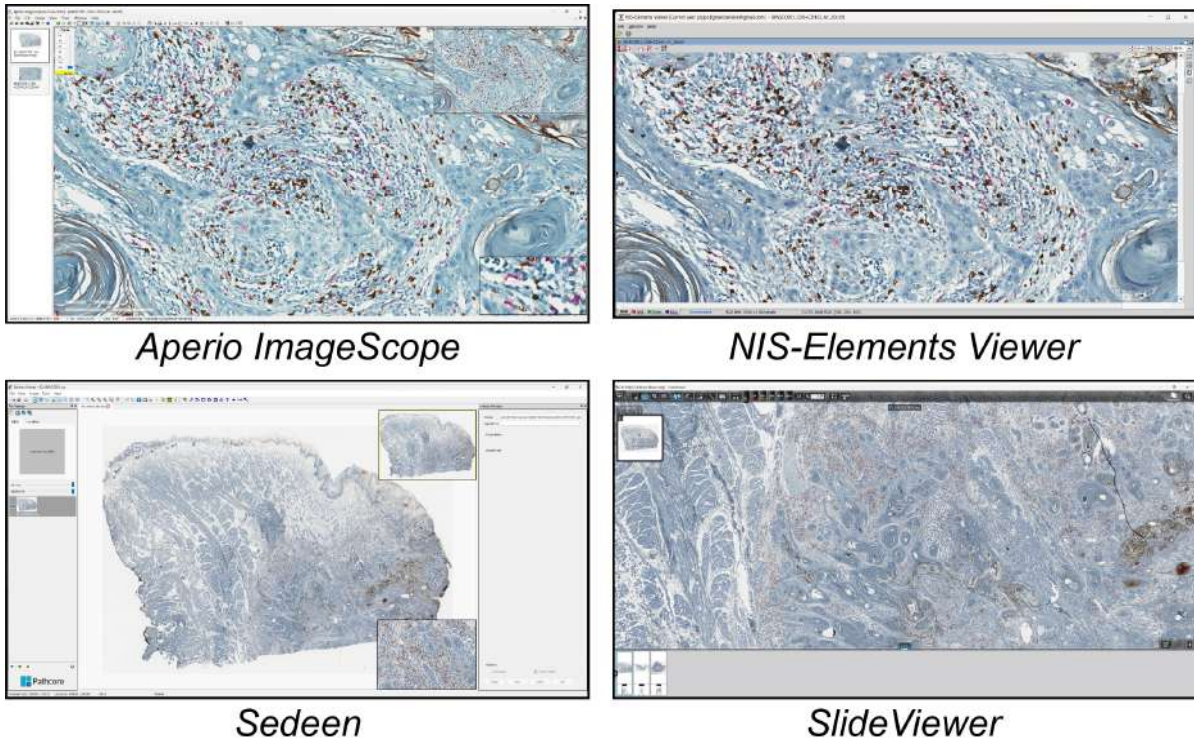


Figure 2. Main GUI of different freely available single-cell analysis tools. From top to bottom and left to right: *Aperio ImageScope*, *NIS-Elements Viewer*, *Sedeen*, and *SlideViewer*.

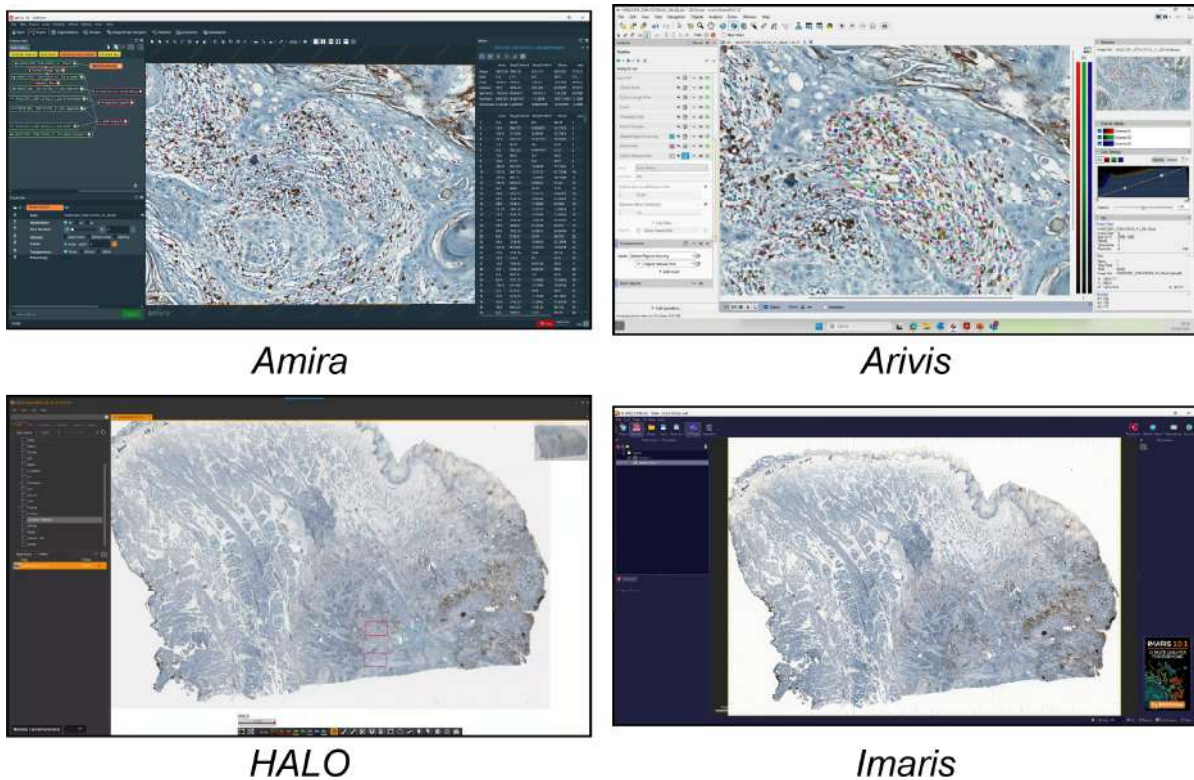


Figure 3. Main GUI of different commercial single-cell analysis tools. From top to bottom and left to right: *Amira*, *Arivis*, *HALO*, and *Imaris*.

Cytomine (<https://cytomine.com/>) [12]: *Cytomine*, originally developed at the University of Liège, offers a cloud-based platform for the collaborative and distributed analysis of WSIs. Unlike *CellProfiler*, it enables multiple users to simultaneously annotate, review, and analyse histological images. In addition, it integrates machine learning opportunities for object detection and cell classification. Its real-time multi-user environment makes it particularly well-suited for projects that involve pathologists, biologists, and data scientists working together, streamlining workflows that require the expert validation of annotations and automated image analysis. *Cytomine* is particularly suited for large datasets due to its web-based nature, allowing the seamless management of WSI data. Its built-in collaborative features make it unique for team-based projects, although its interface and capabilities require more familiarity with information technology (IT) infrastructure. Its image management system comprises a group of image servers and libraries, such as *OpenSlide* [22] to read various WSI formats. The user interface enables communication with other modules via hypertext transfer protocol (HTTP) requests. The data mining module includes clients (e.g., *Python* and *Java*) that provide foundational functions for accessing resources externally within *Cytomine*.

Digital Slide Archive (<https://digitalslidearchive.github.io/>) [13]: *Digital Slide Archive* (DSA) is a highly scalable platform for WSI management, offering robust tools for storing, viewing, and sharing slides across distributed systems. Initially developed at the University of Atlanta, it is based on the *Cancer Digital Slide Archive* (CDSA). While the DSA is primarily focused on WSI management, it includes plugins for exporting ROIs and integrating with other analysis tools, such as *ImageJ* and *QuPath*, to enable further single-cell analysis. Unlike desktop-based software, DSA is designed for high-performance computing environments, enabling the handling of vast repositories of images without performance degradation. The DSA framework consists of several key components: a *Python*-based image processing toolkit for quantitative analysis of digital pathology images, a web-based application for visualising, annotating, and processing histology slides to extract both low- and high-level features, a database layer utilising *MongoDB*, and a web server that offers *RESTful* APIs for programmatic interaction with the DSA. These APIs enable the efficient management of data, user accounts, annotations, and their associated permissions. The platform also incorporates *HistomicsTK* (by Kitware Inc., Clifton Park, NY), a *Python* toolkit that provides a comprehensive set of algorithms for WSI processing and analysis, including pre-processing, segmentation, feature extraction, and other utilities. Additionally, the open-source, web-based *Girder* plugin, built on *OpenSlide*, was developed by Kitware to handle ultra-high-resolution images efficiently.

Icy (<https://icy.bioimageanalysis.org/>) [14]: *Icy*, created in 2011 by the BioImage Analysis Lab at Institut Pasteur, is an extensible, plugin-based platform for image analysis, offering flexibility for a wide range of biological imaging applications, including single-cell analysis. Its strength lies in the integration of a GUI with programming environments (e.g., scripting via *Java* or *Python*), making it accessible to both novice users and developers. The platform provides a visual programming framework, allowing users to design workflows using a drag-and-drop interface, making it easier for non-programmers to build complex analyses. *Icy* is highly modular, with dedicated plugins for cell segmentation, tracking, and fluorescence quantification. Furthermore, *Icy* can be connected to *MATLAB* and provides a native *ImageJ* integration. Its learning curve can be steep for advanced use, and its community and plugin support are smaller compared to more established platforms like *ImageJ*.

ImageJ/Fiji (<https://imagej.net/>) [15,16]: The first version of *ImageJ* was released in 1997 by the National Institutes of Health (NIH, Bethesda, MD, USA), and since then, it has become one of the most widely used programs in the biological field. A wide range of

modules (including plugins and macros) are available, with certain distributions bundling them into single packages. *Fiji* is the most widely used of these distributions, offering hundreds of plugins. *ImageJ* allows users to view, annotate, markup, modify, and analyse different types of biomedical images under *Linux*, *macOS*, and *Windows* operating systems. Today, it is one of the most widely adopted image analysis platform due to its flexibility and extensive plugin ecosystem.

QuPath (<https://qupath.github.io/>) [17]: *QuPath*, developed by Queen's University Belfast, runs on *Linux*, *macOS*, and *Windows* with GUI supported by *JavaFX*. It is created and specifically designed for pathology-driven projects. It has strong support for single-cell quantification and is optimised for large WSI data. *QuPath*'s ability to integrate deep learning models for cell detection and phenotyping gives it a significant advantage over other tools. Its intuitive user interface and support for scripting (in *Groovy* or *JavaScript*) make it both user-friendly and powerful for custom workflows. *QuPath* allows file exchange with *ImageJ* and *MATLAB*. *QuPath* uses Open Microscopy Environment Remote Objects (OMERO) as data storage technology [23].

2.2. Freely Available Tools

Aperio ImageScope (by Leica, <https://www.leicabiosystems.com/>): *Aperio ImageScope* is a Windows-based software application designed for the visualisation, management, and analysis of digital pathology images, particularly WSIs. This tool provides a robust platform for pathologists to interact with high-resolution tissue samples. It offers advanced image rendering capabilities, allowing navigation through large datasets, and annotation tools that facilitate documentation and the communication of diagnostic findings. It supports multiple image formats and integrates with other Leica Biosystems products. Recognized for its speed, it is one of the fastest applications available for viewing and annotating WSI files.

NIS-Elements Viewer (by Nikon, <https://www.microscope.healthcare.nikon.com/>): *NIS-Elements* is a comprehensive commercial imaging software platform that facilitates microscope control, image capture, documentation, image analysis, and data management. The platform includes a free viewer (i.e., *NIS-Elements Viewer*), which supports the display of single images and datasets, offering multiple viewing options such as three-dimensional (3D) *Volume View*. It is optimised for multi-dimensional and time-lapse imaging for dynamic studies where the spatial and temporal analysis of samples is required. *NIS-Elements* also supports macro programming using a C-like language.

Sedeen (by Pathcore, <https://pathcore.com/sedeen>): *Sedeen* is a freely available pathology image viewer developed with support from the Ontario Cancer Research Institute. Designed as a universal platform for the academic community, it facilitates the sharing of digital pathology visualisation and analysis tools with pathologists and imaging researchers. Building in C++ for high computational performance, *Sedeen* integrates smoothly with widely used image analysis libraries, including *ITK* [24], *VTK* [25], and *OpenCV* [26]. It provides researchers with built-in analysis tools and supports the development of custom algorithms for detecting cancerous tissues. The viewer features a simple user interface and exports files in extensible markup language (XML) format.

SlideViewer (by 3DHISTECH, <https://www.3dhistech.com/>): *SlideViewer* (formerly known as *CaseViewer*) is an advanced digital pathology software application for visualising, analysing, and managing WSIs with a user-friendly interface tailored for high-resolution tissue sample exploration. The software offers quantitative image analysis features, facilitating automated assessments of histological parameters. Designed to integrate with other platforms, *SlideViewer* enables workflow management and data sharing, while its compatibility with the 3DHISTECH *eSlide Manager* further supports collaborative case sharing and remote consultations among pathologists and researchers.

2.3. Commercial Tools

Amira (by Thermo Fisher Scientific, <https://www.thermofisher.com/>): *Amira* is an advanced software platform tailored specifically for life science and biomedical research, enabling researchers to work with data from various imaging modalities. It offers advanced data visualisation, image processing, image segmentation, and quantitative analysis tools. Its GUI simplifies complex image-processing tasks by allowing users to visually construct analysis pipelines. This drag-and-drop functionality enhances accessibility for users with limited programming experience while maintaining powerful customisation options for advanced users. The platform supports scripting languages, including *Python* and *MATLAB*.

Arivis (by ZEISS, <https://www.arivis.com/>): *Arivis* is a modular software for scientific image analysis distributed by ZEISS. It enables work with 2D, 3D, and four-dimensional (4D) multichannel images of virtually unlimited size, as datasets are loaded into RAM dynamically based on the data the user views. The software can leverage high-performance computing environments, enabling the parallel processing of image data across multiple computing nodes. *Arivis* offers a highly scalable infrastructure, not dependent on local system resources, enabling it to process and quantify any type of multidimensional image data. Complex analysis can be performed and capabilities for image processing and automatic segmentation using machine learning models and deep learning-based tools can be leveraged. There is also the *Arivis Cloud* platform (formerly known as Apeer), a web-based infrastructure that allows you to leverage image analysis tools via AI using the ZEISS *Arivis* AI toolkit.

HALO (by Indica Labs, <https://indicalab.com/halo/>): *HALO* provides an intuitive and user-friendly interface, even for novice users, enabling analysis without the need to develop algorithms from scratch or configure complex workflows. The application's modular architecture is tailored to meet diverse sample analysis needs, ensuring flexibility, scalability, and high performance. Users can leverage pre-trained deep learning networks for automatic cell segmentation in both brightfield and fluorescence images or train their models through the *HALO* AI module, for example, by using transfer learning methods. *HALO* streamlines the analysis process with a comprehensive set of annotation tools, including freehand drawing and AI-powered functionalities.

Imaris (by Oxford Instruments, <https://imaris.oxinst.com/>): *Imaris* by Oxford Instruments offers a sophisticated platform for the visualisation, segmentation, and quantitative analysis of complex 2D, 3D, and 4D fluorescent images. It is designed for the interactive visualisation, analysis, and interpretation of complex microscopic data. *Imaris* is specifically tailored for managing large, multidimensional datasets derived from widefield fluorescence microscopy, confocal imaging, and other high-resolution techniques such as light-sheet fluorescence microscopy (LSFM [27]). *Imaris* facilitates time-lapse analysis, allowing researchers to study cellular behaviours and morphological changes over time. Additionally, it offers specialised packages designed to meet the needs of various life sciences disciplines. For example, the *Imaris for Cell Biologists* package includes tools for cell segmentation and analysis, supports two-way interfacing with programming languages like *MATLAB*, *Java*, and *Python*, and supports the integration of external software. Nevertheless, *Imaris* is not designed to work with brightfield microscopy images.

3. Qualitative Comparison

Tables 1–3 present a comparative overview of the different tools considered in this work, highlighting key features such as single-cell classification capabilities, ROI flexibility, and file format compatibility. Precisely, Table 1 reports the main characteristics of the six open-source tools considered; Table 2, the four freely available ones; and Table 3, the four

commercial tools. It is worth noting that all selected tools were tested for their compatibility with large histological file formats, including SVS, DICOM, and TIFF, which are commonly used in high-resolution whole-slide imaging. The evaluation specifically focused on each tool's ability to open, visualise, and interact with these formats for the single-cell analysis of stained cells, which are frequently encountered in both clinical and research settings.

Table 1. Open-source tools for single-cell analysis of histological images (X = yes, O = no).

	<i>CellProfiler</i>	<i>Cytomine</i>	<i>Digital Slide Archive</i>	<i>Icy</i>	<i>ImageJ/Fiji</i>	<i>QuPath</i>
VERSION						
Release (year)	2005	2010	2017	2011	1997	2016
Current version	4.2.6	3.2.3	1.1.0	2.5.2	1.54	0.5.0
DOCUMENTATION						
Language	<i>Python</i>	<i>Python, Java</i>	<i>Python</i>	<i>Java</i>	<i>Java</i>	<i>Java</i>
Manual	X	X	X	X	X	X
Website	X	X	X	X	X	X
Open code	X	X	X	X	X	X
USABILITY						
SVS/DICOM/TIFF	X/X/X	X/X/X	X/O/X	X/X/X	X/X/X	X/X/X
Supporting 3D data	X (plugin)	O	O	X	X (plugin)	O
Programming skills request	X	O	O	O	O	O
GUI user-friendly	O	X	X	X	X	X
Multiplatform	X	X	O	X	X	X
FUNCTIONALITY						
ROI importing	X (mask)	O	O	X (.xml)	X (mask)	X (GeoJSON)
ROI exporting	X (mask)	O	O	X (.xml)	X (mask)	X (GeoJSON)
Automatic segmentation	X	X	X	X (plugin)	X (plugin)	X
Manual segmentation	X	X	X	X	X	X
Semiautomatic segmentation	X	X	X	X	X	X
Automatic classification	X	X	O	X (plugin)	X (plugin)	X
Manual classification	X	X	X	X	X	X
Extensibility	X	X	X	X	X	X

Table 2. Freely available tools for single-cell analysis of histological images (X = yes, O = no).

	<i>Aperio ImageScope</i>	<i>NIS-Elements Viewer</i>	<i>Sedeen</i>	<i>SlideViewer</i>
VERSION				
Release (year)	2011	2007	2013	2012
Current version	12.4.6	5.21.00	5.4.4	2.7
DOCUMENTATION				
Language	C++	C++	//	C++
Manual	X	X	X	X
Website	X	X	X	X
Open code	O	O	O	O
USABILITY				
SVS/DICOM/TIFF	X/O/X	O/O/X	X/O/X	X/X/X
Supporting 3D data	O	X	O	X
Programming skills request	O	O	O	O
GUI user-friendly	X	X	X	X
Multiplatform	Windows only	X	Windows only	X
FUNCTIONALITY				
ROI importing	O	O	O	O
ROI exporting	O	O	O	O
Automatic segmentation	O	O	O	O
Manual segmentation	X	O	X	X
Semiautomatic segmentation	O	O	O	O
Automatic classification	O	O	O	O
Manual classification	O	O	O	X
Extensibility	O	O	X	O

Table 3. Commercial tools for single-cell analysis of histological images (X = yes, O = no).

	<i>Amira</i>	<i>Arivis</i>	<i>HALO</i>	<i>Imaris</i>
VERSION				
Release (year)	1999	2002	2012	1993
Current version	2023.2	4.1.2	4.0	10.1
DOCUMENTATION				
Language	//	//	C++	//
Manual	X	X	X	X
Website	X	X	X	X
Open code	O	O	O	O
USABILITY				
SVS/DICOM/TIFF	O/X/X	X/X/X	X/X/X	X/X/X

Table 3. Cont.

	<i>Amira</i>	<i>Arivis</i>	<i>HALO</i>	<i>Imaris</i>
Supporting 3D data	X	X	O	X
Programming skills request	O	O	O	O
GUI user-friendly	X	X	X	X
Multiplatform	X	Windows only	X	X
FUNCTIONALITY				
ROI importing	X (mask)	X (mask)	X	X
ROI exporting	X (mask)	X (mask)	X	X
Automatic segmentation	X	X	X	X
Manual segmentation	O	X	X	O
Semiautomatic segmentation	X	O	X	O
Automatic classification	X	X	X	X
Manual classification	O	O	X	O
Extensibility	O	X (<i>Python</i> , <i>MATLAB</i>)	O	X

4. Quantitative Comparison

In order to evaluate the performance of the different tools, (a) the total number of cells and (b) the number of cells positive to some specific markers within a specific irregular freehand-defined ROI of a representative brightfield image (Figure 4a) were counted using the different tools.

The freehand-defined ROI (Figure 4b) was defined on an extracted 2346×1352 full-resolution rectangular image within a large high-resolution WSI of an anonymised IHC-stained tissue section of a head and neck squamous cell carcinoma (HNSCC) tumour biopsy, precisely, a tongue cancer, used as a sample dataset (Figure 4c). The image was acquired using a brightfield *Aperio CS2* microscope (*Leica Biosystems*), equipped with a $40\times$ objective. The section was stained using three different markers: nuclei are stained with haematoxylin (visible in blue), CD8-positive lymphocytes with DAB (*3,3'-Diaminobenzidine*, visible in brown), and CD163-positive macrophages with AP-red (*Alkaline Phosphatase Red*, visible in red). Haematoxylin (Figure 4d), DAB (Figure 4e), and AP-red (Figure 4f) channels were extracted and saved as different image files using the *Colour Deconvolution* tool, an *ImageJ/Fiji* plugin for stain unmixing in RGB histological images [28].

The representative rectangular image extracted from the WSI file, the binary mask representing the irregular freehand-defined ROI, the haematoxylin image, the DAB image, and the AP-red image are freely available as Supplementary File S1.

The ground truth was established by an expert life scientist who manually counted the total number of cells (i.e., 823), as well as the number of cells positive for DAB (i.e., 135) and AP-red (i.e., 98) within the irregular freehand-defined ROI. Each tool was then tested by the same operator, an expert computer scientist, using the same previously freehand-defined ROI saved and loaded into the different tools. It is worth noting that the computer scientist testing the tools was trained by the life scientist responsible for creating the ground truth, learning to recognise cellular structures and identify various staining signals on ROIs similar to, but different from, the one used in the experiments.

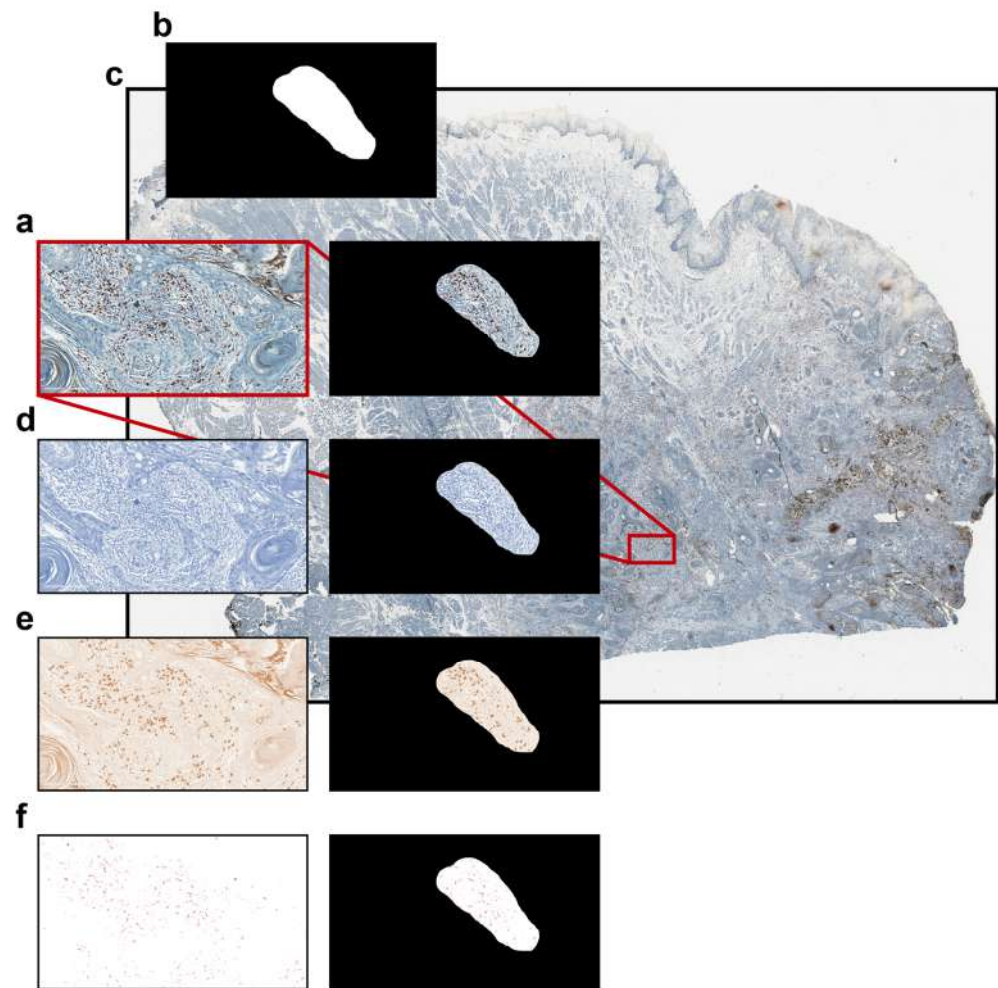


Figure 4. Brightfield dataset used for comparing the different single-cell analysis tools. (a) Representative brightfield RGB image; (b) binary mask representing an irregular freehand-defined ROI; (c) original high-resolution WSI file with the position of the extracted image highlighted in red; (d) haematoxylin-channel image; (e) DAB-channel image; and (f) AP-red-channel image.

All the tools unable to load the previously defined irregular freehand-defined ROI or unable to detect cells stained with DAB and/or AP-red were discarded, remaining just: (1) *Amira*, (2) *Arivis*, (3) *HALO*, (4) *ImageJ/Fiji*, (5) *NIS-Elements* (in this case we did not use *NIS-Elements Viewer* but its commercial version *NIS-Elements* with several segmentation and classification functionalities), (6) *QuPath*. The tested tools were installed on a workstation with the following configuration: an Intel Core i7 processor, 32 gigabyte (GB) random access memory (RAM), and NVIDIA GTX 1080 graphics card. Software packages were obtained from official sources, with open-source and freely-available tools downloaded from their respective websites on May 2024, while commercial tools were tested using trial time-limited licenses provided by vendors. Setups were completed by following the user manuals or installation guides, ensuring that all necessary dependencies and configurations were met for each software.

5. Results and Discussion

Among the 14 tools initially reviewed, only six met the requirements for the experiments: They supported loading the predefined irregular freehand-selected ROI and analysing both nuclear (i.e., haematoxylin) and cellular (i.e., DAB and AP-red) signals. Precisely, the tools considered in the experiments were (hereafter reported in alphabetical or-

der) (1) *Amira* (commercial), (2) *Arivis* (commercial), (3) *HALO* (commercial), (4) *ImageJ/Fiji* (open source), (5) *NIS-Elements* (commercial version of the freely available *NIS-Elements Viewer*, including options for importing image ROIs and performing automatic single-cell segmentation/classification), and (6) *QuPath* (open source). What follows summarises the parameters applied and strategy used for testing the following single-cell analysis software tools (hereafter reported in alphabetical order):

(1) *Amira*: *Amira* is a commercial tool, and the testing was conducted using a license provided by the selling company for a limited evaluation period. Accordingly, the reported values can be considered a lower bound, with potential for improvements. For the segmentation, we analysed the haematoxylin, DAB, and AP-red images separately. A basic global thresholding step was followed by the application of the standard *Watershed* algorithm to segment and split objects, as well as to remove small debris. The key internal parameters applied during the process were as follows: threshold range, 0–120 grey levels; Watershed option, *DARK*; global segmentation range, 1.00–6.75; segmentation level, 0.6; and minimum object area, 30 pixels.

(2) *Arivis*: *Arivis* is a commercial tool, and the testing was conducted in collaboration with specialists from ZEISS, the selling company, through an online meeting aimed at ensuring proper usage of the software. This collaborative effort allowed us to apply the tool to brightfield images as effectively as possible while acknowledging that the tool was primarily developed for fluorescent images. However, the limited time of interaction with the specialists made the reported values just a lower bound with a high potential for improvements. For instance, pre-training specific networks could obviously provide better accuracy. For the segmentation, we separately considered the haematoxylin, DAB, and AP-red images. Built-in machine learning algorithms originally validated for fluorescent images and not optimised for brightfield applications were used. Following segmentation, the internal *Blob Finder* algorithm was used to count both nuclei and cells with positive signals. The preliminary results were further refined by applying area and circularity filters to reduce false positives and debris.

(3) *HALO*: *HALO* is a commercial tool, and the testing was conducted in collaboration with specialists from Indica Labs, the selling company, through an online meeting to ensure proper usage and application of the software. This collaborative effort enabled us to apply the tool to brightfield images as effectively as possible while acknowledging that the tool was primarily developed for fluorescent image analysis. However, the limited time of interaction with the specialists made the reported values just a lower bound with a high potential for improvements. For segmentation, we analysed the haematoxylin, DAB, and AP-red images separately. An available pre-trained neural network, optimised for images similar to the haematoxylin stain, was used for nuclei segmentation, yielding extremely highly accurate results. However, no available neural networks had been trained on images resembling the DAB and AP-red stains, resulting in very poor accuracy when identifying cells positive for these markers. Obviously, specific pre-trained networks could provide better accuracy.

(4) *ImageJ/Fiji*: *ImageJ/Fiji* is an open-source tool providing several image processing options and plugins. For the segmentation, we separately considered the haematoxylin, DAB, and AP-red images. Each image has been converted into a binary mask applying a basic global thresholding step, followed by the application of the standard *Watershed* algorithm to segment and split objects, as well as to remove small debris. Finally, the *Particle Analysis* plugin was used for counting the objects. The key internal parameters applied during the process were as follows: threshold range, 0–175 grey levels; circularity, 0.00–1.00; minimum object area, 60 pixels; and removal of the objects touching borders, *Yes*.

(5) *NIS-Elements*: *NIS-Elements* is a commercial tool, and the testing was conducted using a license acquired by the selling company. *NIS-Elements* provides several image processing options. For the segmentation, we separately considered the haematoxylin, DAB, and AP-red images. Each image has been converted into a binary mask by applying a basic global thresholding step, followed by the application of internal built-in filters for smoothing the images, separating objects, and removing small debris. The key internal parameters applied during the process were as follows: threshold range, 0–225 grey levels; smooth, 2x; separate, 2x; clean, 2x; all filling, No.

(6) *QuPath*: *QuPath* is an open-source tool providing several image processing options and macros. It also provides automatic neural networks and options for different microscopy image classes, including specific opportunities for histological brightfield images. For the segmentation, we just considered the original rectangular RGB image. In particular, it was processed using an automatic segmentation option available for brightfield images, providing as output both the single-nucleus and the single-cell segmentations. Those segmentations have been then analysed using a supervised classification neural network available for counting the number of nuclei and the number of DAB- and AP-red-positive cells within the irregular freehand-defined ROI. The key internal parameters applied during the process were as follows: pixel size, 0.5 μm ; nuclear background radius, 8 μm ; median filter radius, 0 μm ; sigma, 1.5 μm ; minimum nuclear area, 8 μm^2 ; maximum nuclear area, 400 μm^2 ; threshold value, 0.1; maximum background intensity, 2.0; and cellular expansion, 5 μm .

The other eight tools were excluded for specific reasons. *Aperio ImageScope* (freely available), *Sedeen* (freely available), and *SlideViewer* (freely available) lacked semi- and fully-automatic classification functionalities. *CellProfiler* (open source), *Cytomine* (open source), *Digital Slide Archive* (open source), and *Icy* (open source) failed to import the irregular freehand-defined ROI or required advanced preprocessing of the input image, unsuitable for a fair comparison of the different tools. *Imaris* (commercial), full of opportunities for fluorescent imaging, lacks segmentation methods for brightfield images.

Figure 5 shows the segmentations obtained using the different tools in a real case study.

Tables 4–7 report the counts, the absolute normalized difference percentage (*PAND*), and the rank position obtained by the different tools when analysing the signals in the preselected irregular freehand-defined ROI. The *PAND* between value (V_i) recorded by the tool (i) and ground truth (G), was computed to measure the closeness of agreement of the different counts according to Equation (1) [29]:

$$PAND = 100 \times |V_i - G| / G \quad (1)$$

Table 4 reports the number of nuclei counted considering the haematoxylin signal, Table 5 reports the number of DAB positive cells, Table 6 reports the number of AP-red positive cells, and Table 7 reports the mean *PAND* and the final rank obtained by averaging together the single *PAND*s computed for the three different signals (i.e., haematoxylin, DAB, and AP-red).

The results reported in Table 4 demonstrate that for nuclei counting using the haematoxylin signal, most tools performed exceptionally well, with a *PAND* below 10%, except for *Arivis*, which showed a higher error rate. Notably, *QuPath* and *HALO* achieved the highest accuracy, with *PAND* values close to 1%. This strong performance is due to segmentation algorithms specifically optimised for nuclei detection in haematoxylin-stained images, a common benchmark for many tools. In general, the relatively low variability across tools reflects the maturity of algorithms for this task, as haematoxylin staining provides strong contrast and clear boundaries for nuclei segmentation. In contrast, the results in Tables 5 and 6 highlight the greater challenge of accurately detecting specific cellular markers, such as DAB and AP-red. For these markers, *PAND* values were generally higher, often exceeding 10%, indicating a

notable decrease in accuracy compared to nuclei counting. Among the evaluated tools, *QuPath* consistently stood out, achieving robust detection capabilities with *PAND* values around 5% for both markers. This suggests that *QuPath*'s segmentation and classification algorithms are better adapted to handling the variability and complexity of brightfield image data, which is less uniform and more prone to staining inconsistencies than fluorescence-based imaging. Lastly, the summary in Table 7 underscores the limitations of certain tools, particularly *Arivis* and *HALO*, which exhibited average *PAND* values exceeding 20%. This underperformance is attributed to the segmentation and classification models implemented in these tools, which are pre-trained and optimised for fluorescence imaging applications. These models struggle to generalise effectively to brightfield images, which involve different optical characteristics, such as variations in illumination and colourimetric dependencies. This highlights a broader challenge in adapting tools initially designed for one imaging modality to another, emphasising the importance of algorithm flexibility and data-driven optimization. In addition, it is important to remember that evaluating the commercial tools was challenging due to the restricted functionality of the testing license. For instance, it was not possible to pre-train specific neural networks for the analysed signals as it was possible to do in *QuPath*. As such, the reported performance values represent a baseline, with potential for improvements.

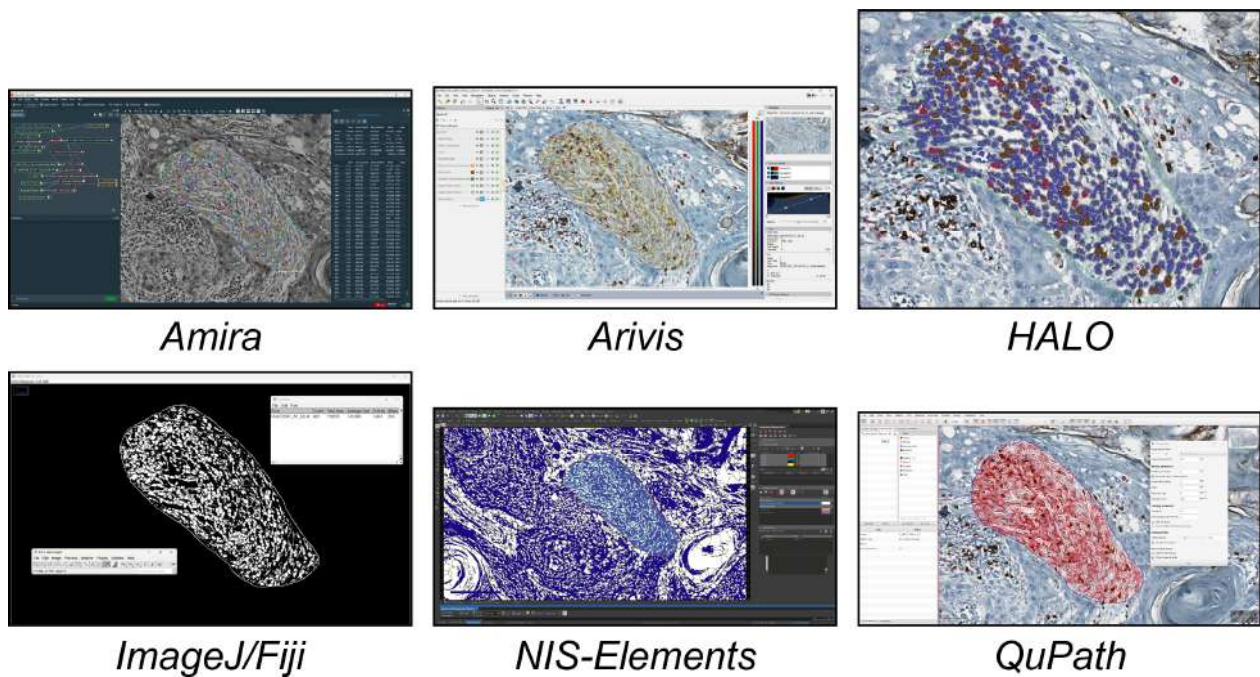


Figure 5. Overview of the segmentations obtained using the different tools. From top to bottom and left to right: *Amira*, *Arivis*, *HALO*, *ImageJ/Fiji*, *NIS-Elements*, and *QuPath*.

Table 4. Haematoxylin analysis.

Software	Count	PAND	Rank
Ground Truth	823	//	//
<i>Amira</i>	871	5.83%	5
<i>Arivis</i>	645	21.62%	6
<i>HALO</i>	815	0.97%	1
<i>ImageJ/Fiji</i>	802	2.55%	3
<i>NIS-Elements</i>	796	3.28%	4
<i>QuPath</i>	832	1.09%	2

Table 5. DAB analysis.

Software	Count	PAND	Rank
<i>Ground Truth</i>	135	//	//
<i>Amira</i>	158	17.03%	4
<i>Arivis</i>	168	24.44%	5
<i>HALO</i>	94	30.37%	6
<i>ImageJ/Fiji</i>	113	16.30%	3
<i>NIS-Elements</i>	128	5.18%	1–2
<i>QuPath</i>	142	5.18%	1–2

Table 6. AP-red analysis.

Software	Count	PAND	Rank
<i>Ground Truth</i>	98	//	//
<i>Amira</i>	113	15.31%	4
<i>Arivis</i>	120	22.45%	5
<i>HALO</i>	51	47.96%	6
<i>ImageJ/Fiji</i>	89	9.18%	2
<i>NIS-Elements</i>	87	11.22%	3
<i>QuPath</i>	101	3.06%	1

Table 7. Mean PAND and final rank.

Software	PAND	Rank
<i>Amira</i>	12.72%	4
<i>Arivis</i>	22.84%	5
<i>HALO</i>	26.43%	6
<i>ImageJ/Fiji</i>	9.34%	3
<i>NIS-Elements</i>	6.56%	2
<i>QuPath</i>	3.11%	1

6. Conclusions and Perspectives

In this work, we reviewed and compared the software currently available for performing single-cell analysis of histological brightfield images. Specifically, we focused on tools capable of analysing stained cells within irregular freehand-defined ROIs. In total, we considered 14 tools (six open-source, four freely available, and four commercial ones) and we practically compared six of them by performing a case study using a representative brightfield dataset.

The results of this comparative analysis revealed that even the open-source tools are today characterised by comprehensive feature sets, which rival those of commercial software solutions. In particular, *QuPath* demonstrated flexibility in handling large file formats, along with robust options for ROI definition and single-cell classification. In contrast, the commercial solutions offered more advanced automation features but lacked the versatility and cost-effectiveness of some open-source tools. This comparison highlights the trade-offs between accessibility and functionality, with *QuPath* emerging as a balanced option for single-cell analysis within histological brightfield images.

To promote future benchmarking, the image dataset and the freehand-defined ROI used in the comparison have been shared as Supplementary Materials to be used by the research community to conduct future comparative analyses of new tools for single-cell analysis in histological brightfield images. It is worth remarking that fluorescent images were out of our interest and the analysis has been limited to cell counting within a single brightfield ROI. The accuracy of the segmentation masks for detected cells was not evaluated, nor was the reproducibility of multiple determinations assessed. Consequently, this evaluation does not provide insights into the precision or reliability of the cell segmentation process. Future work will involve a more detailed analysis of the segmentation masks, including an assessment of false positives and false negatives. Additionally, several tools were excluded (e.g., *Imaris*) or delivered suboptimal results (e.g., *Arivis*) due to their lack of segmentation methods trained for brightfield images, despite their strong performance with fluorescent ones. In future, the experiments may be extended to WSI acquired with motorised fluorescent confocal microscopes to provide a more comprehensive assessment of the tools also in different specific cases. Eventually, the tests could also be extended to monitor how different tools handle various image types. For instance, we currently consider the most popular format, i.e., RGB, but multi-channel images with more than three channels are becoming increasingly common and could also be included [30]. Finally, the experiments in this study were conducted by an expert in computer science. However, future work could benefit from incorporating usability feedback from less experienced users, such as an early-career life scientist. Nevertheless, this work offers a deeper understanding of the strengths and limitations of various software platforms, facilitating more informed decision making for researchers seeking tools to analyse histological brightfield images and paving the way for further insights.

Supplementary Materials: The following supporting information can be downloaded at <https://www.mdpi.com/article/10.3390/technologies13030110/s1>. File S1: Brightfield dataset for comparing the different single-analysis tools. Representative image (*HNSCC001_CD8_CD163_H.tif*) extracted from a high-resolution WSI of an anonymised IHC-stained tissue section of a head and neck squamous cell carcinoma (HNSCC) tumour biopsy, precisely, a tongue cancer. The image was acquired using a brightfield *Aperio CS2* microscope (*Leica Biosystems*), equipped with a 40× objective. The section was stained using 3 different markers: nuclei are stained with haematoxylin (visible in blu), CD8-positive lymphocytes with DAB (*3,3'-Diaminobenzidine*, visible in brown), and CD163-positive macrophages with AP-red (*Alkaline Phosphatase Red*, visible in red). The three single-channel images (*HNSCC001_H.tif*, *HNSCC001_CD8.tif*, *HNSCC001_CD163.tif*) obtained using the *Colour Deconvolution* tool are here provided with the 2D binary mask (*BinaryMask.tif*) representing a user irregular freehand-defined ROI.

Author Contributions: Conceptualisation: F.P., M.T., and A.C.; Methodology: F.P., M.T., M.M.T., N.N., and A.C.; Software: F.P., G.C., and A.C.; Validation: F.P., M.T., M.M.T., and A.C.; Formal analysis: F.P., M.T., M.M.T., and A.C.; Investigation: F.P., M.T., M.M.T., and A.C.; Resources: F.P., N.N., G.C., and A.C.; Data curation: F.P., M.T., and M.M.T.; Writing—original draft preparation: F.P., M.T., and A.C.; Writing—review and editing: M.M.T., N.N., and G.C.; Visualisation: F.P., M.T., and M.M.T.; Supervision: N.N., G.C., and A.C.; Project administration: F.P. and A.C.; Funding acquisition: F.P., N.N., G.C., and A.C. All authors have read and agreed to the published version of the manuscript.

Funding: M.T. acknowledges support from the “Associazione Italiana per la Ricerca sul Cancro” (grant no. MFAG 2021—ID. 26339). N.N. acknowledges support from the Italian Ministry of Health and the contribution of “Ricerca Corrente” within the research line “Appropriateness, outcomes, drug value and organisational models for the continuity of diagnostic therapeutic pathways in oncology”. F.P. acknowledges support from the European Union—NextGenerationEU through the Italian Ministry of University and Research under PNRR—M4C2-I1.3 Project PE_00000019 “HEAL ITALIA” (CUP: J33C22002920006); G.C. under PNRR—INF-ACT Project PE13 “One Health Ba-

sic and Translational Actions Addressing Unmet Needs on Emerging Infectious Diseases” (CUP: J33C22002870005); A.C. under PNRR—PNC Project PNC0000002 “DARE—Digital Lifelong Prevention” (CUP: B53C22006240001). It is worth noting that the views and opinions expressed are those of the authors only and do not necessarily reflect those of the European Union or the European Commission. Neither the European Union nor the European Commission can be held responsible for them.

Institutional Review Board Statement: Not applicable.

Informed Consent Statement: Not applicable.

Data Availability Statement: The image and mask used in this study are available as Supplementary Materials.

Acknowledgments: The authors would like to thank Filippo Pilutti (DISI, University of Bologna, Italy) and Mariachiara Stellato (DIFA, University of Bologna) for their contributions to the tool testing process.

Conflicts of Interest: The authors declare that have no competing interests.

Abbreviations

2D	Two-dimensional
3D	Three-dimensional
4D	Four-dimensional
AI	Artificial intelligence
CDSA	Cancer digital slide archive
DICOM	Digital imaging and communications in medicine
DL	Deep learning
DSA	Digital slide archive
GB	Gigabyte
GUI	Graphical user interface
HNSCC	Head and neck squamous cell carcinoma
HTTP	Hypertext transfer protocol
IHC	Immunohistochemistry
IT	Information technology
LSFM	Light-sheet fluorescent microscopy
NIH	National Institutes of Health
OMERO	Open microscopy environment remote objects
PAND	Absolute normalised difference percentage
RAM	Random access memory
RGB	Red, green, blue
ROI	Regions of interest
SVS	Scanner vendor-specific format
TIFF	Tagged image file format
WSI	Whole slide imaging
XML	Extensible markup language

References

1. Hosseini, M.S.; Bejnordi, B.E.; Trinh, V.Q.-H.; Chan, L.; Hasan, D.; Li, X.; Yang, S.; Kim, T.; Zhang, H.; Wu, T.; et al. Computational pathology: A survey review and the way forward. *J. Pathol. Inform.* **2024**, *15*, 100357. [[CrossRef](#)] [[PubMed](#)]
2. Wu, Y.; Cheng, M.; Huang, S.; Pei, Z.; Zuo, Y.; Liu, J.; Yang, K.; Zhu, Q.; Zhang, J.; Hong, H.; et al. Recent advances of deep learning for computational histopathology: Principles and applications. *Cancers* **2022**, *14*, 1199. [[CrossRef](#)]
3. Parra, E.R.; Ilié, M.; Wistuba, I.I.; Hofman, P. Quantitative multiplexed imaging technologies for single-cell analysis to assess predictive markers for immunotherapy in thoracic immuno-oncology: Promises and challenges. *Br. J. Cancer* **2023**, *129*, 1417–1431. [[CrossRef](#)]

4. Jain, E.; Patel, A.; Parwani, A.V.; Shafi, S.; Brar, Z.; Sharma, S.; Mohanty, S.K. Whole slide imaging technology and its applications: Current and emerging perspectives. *Int. J. Surg. Pathol.* **2024**, *32*, 433–448. [[CrossRef](#)]
5. Pavone, A.M.; Giannone, A.G.; Cabibi, D.; D'aprile, S.; Denaro, S.; Salvaggio, G.; Parenti, R.; Yezzi, A.; Comelli, A. Digital Pathology: A Comprehensive Review of Open-Source Histological Segmentation Software. *BioMedInformatics* **2024**, *4*, 173–196. [[CrossRef](#)]
6. Xun, D.; Wang, R.; Zhang, X.; Wang, Y. Microsnoop: A generalist tool for microscopy image representation. *Innov.* **2024**, *5*, 100541. [[CrossRef](#)]
7. Vanea, C.; Džigurski, J.; Rukins, V.; Dodi, O.; Siigur, S.; Salumäe, L.; Meir, K.; Parks, W.T.; Hochner-Celnikier, D.; Fraser, A.; et al. Mapping cell-to-tissue graphs across human placenta histology whole slide images using deep learning with HAPPY. *Nat. Commun.* **2024**, *15*, 2710. [[CrossRef](#)]
8. Guerrero, R.E.D.; Carvalho, L.; Bocklitz, T.; Popp, J.; Oliveira, J.L. Software tools and platforms in Digital Pathology: A review for clinicians and computer scientists. *J. Pathol. Inform.* **2022**, *13*, 100103. [[CrossRef](#)] [[PubMed](#)]
9. Ali, M.; Benfante, V.; Basirinia, G.; Alongi, P.; Sperandeo, A.; Quattrocchi, A.; Giannone, A.G.; Cabibi, D.; Yezzi, A.; Di Raimondo, D.; et al. Applications of Artificial Intelligence, Deep Learning, and Machine Learning to Support the Analysis of Microscopic Images of Cells and Tissues. *J. Imaging* **2025**, *11*, 59. [[CrossRef](#)]
10. Piccinini, F.; Balassa, T.; Szkalitsity, A.; Molnar, C.; Paavolainen, L.; Kujala, K.; Buzas, K.; Sarazova, M.; Pietiainen, V.; Kutay, U.; et al. Advanced cell classifier: User-friendly machine-learning-based software for discovering phenotypes in high-content imaging data. *Cell Syst.* **2017**, *4*, 651–655.e5. [[CrossRef](#)]
11. Stirling, D.R.; Swain-Bowden, M.J.; Lucas, A.M.; Carpenter, A.E.; Cimini, B.A.; Goodman, A. CellProfiler 4: Improvements in speed, utility and usability. *BMC Bioinform.* **2021**, *22*, 433. [[CrossRef](#)] [[PubMed](#)]
12. Marée, R.; Rollus, L.; Stévens, B.; Hoyoux, R.; Louppe, G.; Vandaele, R.; Begon, J.-M.; Kainz, P.; Geurts, P.; Wehenkel, L. Collaborative analysis of multi-gigapixel imaging data using Cytomine. *Bioinformatics* **2016**, *32*, 1395–1401. [[CrossRef](#)] [[PubMed](#)]
13. Gutman, D.A.; Khalilia, M.; Lee, S.; Nalisnik, M.; Mullen, Z.; Beezley, J.; Chittajallu, D.R.; Manthey, D.; Cooper, L.A. The digital slide archive: A software platform for management, integration, and analysis of histology for cancer research. *Cancer Res.* **2017**, *77*, e75–e78. [[CrossRef](#)] [[PubMed](#)]
14. de Chaumont, F.; Dallongeville, S.; Chenouard, N.; Hervé, N.; Pop, S.; Provoost, T.; Meas-Yedid, V.; Pankajakshan, P.; Lecomte, T.; Le Montagner, Y.; et al. Icy: An open bioimage informatics platform for extended reproducible research. *Nat. Methods* **2012**, *9*, 690–696. [[CrossRef](#)]
15. Schindelin, J.; Rueden, C.T.; Hiner, M.C.; Eliceiri, K.W. The ImageJ ecosystem: An open platform for biomedical image analysis. *Mol. Reprod. Dev.* **2015**, *82*, 518–529. [[CrossRef](#)]
16. Schindelin, J.; Arganda-Carreras, I.; Frise, E.; Kaynig, V.; Longair, M.; Pietzsch, T.; Preibisch, S.; Rueden, C.; Saalfeld, S.; Schmid, B.; et al. Fiji: An open-source platform for biological-image analysis. *Nat. Methods* **2012**, *9*, 676–682. [[CrossRef](#)]
17. Bankhead, P.; Loughrey, M.B.; Fernández, J.A.; Dombrowski, Y.; McArt, D.G.; Dunne, P.D.; McQuaid, S.; Gray, R.T.; Murray, L.J.; Coleman, H.G.; et al. QuPath: Open source software for digital pathology image analysis. *Sci. Rep.* **2017**, *7*, 16878. [[CrossRef](#)]
18. Fassler, D.J.; Abousamra, S.; Gupta, R.; Chen, C.; Zhao, M.; Paredes, D.; Batool, S.A.; Knudsen, B.S.; Escobar-Hoyos, L.; Shroyer, K.R.; et al. Deep learning-based image analysis methods for brightfield-acquired multiplex immunohistochemistry images. *Diagn. Pathol.* **2020**, *15*, 100. [[CrossRef](#)]
19. Morrison, L.E.; Lefever, M.R.; Behman, L.J.; Leibold, T.; Roberts, E.A.; Horchner, U.B.; Bauer, D.R. Brightfield multiplex immunohistochemistry with multispectral imaging. *Laboratory Investigation.* **2020**, *100*, 1124–1136. [[CrossRef](#)]
20. Rehák, R.; Bodrogi, P.; Schanda, J. On the use of the sRGB colour space. *Displays* **1999**, *20*, 165–170. [[CrossRef](#)]
21. Carpenter, A.E.; Jones, T.R.; Lamprecht, M.R.; Clarke, C.; Kang, I.H.; Friman, O.; Guertin, D.A.; Chang, J.H.; Lindquist, R.A.; Moffat, J.; et al. CellProfiler: Image analysis software for identifying and quantifying cell phenotypes. *Genome Biol.* **2016**, *7*, R100. [[CrossRef](#)] [[PubMed](#)]
22. Goode, A.; Gilbert, B.; Harkes, J.; Jukic, D.; Satyanarayanan, M. OpenSlide: A vendor-neutral software foundation for digital pathology. *J. Pathol. Inform.* **2013**, *4*, 27. [[CrossRef](#)] [[PubMed](#)]
23. Allan, C.; Burel, J.-M.; Moore, J.; Blackburn, C.; Linkert, M.; Loynton, S.; MacDonald, D.; Moore, W.J.; Neves, C.; Patterson, A.; et al. OMERO: Flexible, model-driven data management for experimental biology. *Nat. Methods* **2012**, *9*, 245–253. [[CrossRef](#)]
24. Bitter, I.; Van Uiter, R.; Wolf, I.; Ibanez, L.; Kuhnigk, J.-M. Comparison of four freely available frameworks for image processing and visualization that use ITK. *IEEE Trans. Vis. Comput. Graph.* **2007**, *13*, 483–493. [[CrossRef](#)] [[PubMed](#)]
25. Geveci, B.; Schroeder, W.; Brown, A.; Wilson, G.V. The architecture of open source applications. *Researchgate* **2012**, *1*, 387–402.
26. Culjak, I.; Abram, D.; Pribanic, T.; Dzapov, H.; Cifrek, M. A brief introduction to OpenCV. In Proceedings of the 2012 Proceedings of the 35th International Convention MIPRO, Opatija, Croatia, 21–25 May 2012; IEEE: Piscataway, NJ, USA, 2012; pp. 1725–1730.
27. Stelzer, E.H.; Strobl, F.; Chang, B.J.; Preusser, F.; Preibisch, S.; McDole, K.; Fiolka, R. Light sheet fluorescence microscopy. *Nat. Rev. Methods Primers* **2021**, *1*, 73. [[CrossRef](#)]

28. Landini, G.; Martinelli, G.; Piccinini, F. Colour deconvolution: Stain unmixing in histological imaging. *Bioinformatics* **2020**, *37*, 1485–1487. [[CrossRef](#)]
29. Piccinini, F.; Martinelli, G.; Carbonaro, A. Accuracy of mobile applications versus wearable devices in long-term step measurements. *Sensors* **2020**, *20*, 6293. [[CrossRef](#)]
30. Piccinini, F.; Tazzari, M.; Tumedei, M.M.; Stellato, M.; Remondini, D.; Giampieri, E.; Martinelli, G.; Castellani, G.; Carbonaro, A. Data Science for Health Image Alignment: A User-Friendly Open-Source ImageJ/Fiji Plugin for Aligning Multimodality/Immunohistochemistry/Immunofluorescence 2D Microscopy Images. *Sensors* **2024**, *24*, 451. [[CrossRef](#)]

Disclaimer/Publisher’s Note: The statements, opinions and data contained in all publications are solely those of the individual author(s) and contributor(s) and not of MDPI and/or the editor(s). MDPI and/or the editor(s) disclaim responsibility for any injury to people or property resulting from any ideas, methods, instructions or products referred to in the content.